Published in final edited form as:
Traffic. 2013 December ; 14(12): . doi:10.1111/tra.12118.

Automated quantification of the subcellular localization of multi-compartment proteins via Q-SCAn

Nicholas C. Bauer[1,2], **Anita H. Corbett**[1,3,*], and **Paul W. Doetsch**[1,3,4,5,*]

[1]Department of Biochemistry, Emory University School of Medicine, Atlanta, GA, 30322, USA

[2]Graduate Program in Biochemistry, Cell, and Developmental Biology, Emory University School of Medicine, Atlanta, GA, 30322, USA

[3]Winship Cancer Institute, Emory University School of Medicine, Atlanta, GA, 30322, United States

[4]Department of Radiation Oncology, Emory University School of Medicine, Atlanta, GA, 30322, United States

[5]Department of Hematology and Medical Oncology, Emory University School of Medicine, Atlanta, GA, 30322, United States

Abstract

In eukaryotic cells, proteins can occupy multiple intracellular compartments and even move between compartments to fulfill critical biological functions or respond to cellular signals. Examples include transcription factors that reside in the cytoplasm but are mobilized to the nucleus as well as dual-purpose DNA repair proteins that are charged with simultaneously maintaining the integrity of both the nuclear and mitochondrial genomes. While numerous methods exist to study protein localization and dynamics, automated methods to quantify the relative amounts of proteins that occupy multiple subcellular compartments have not been extensively developed. To address this need, we present a rapid, automated method termed Quantitative Subcellular Compartmentalization Analysis (Q-SCAn). To develop this method, we exploited the facile molecular biology of the budding yeast, *Saccharomyces cerevisiae*. Individual subcellular compartments are defined by a fluorescent marker protein and the intensity of a target GFP-tagged protein is then quantified within each compartment. To validate Q-SCAn, we analyzed relocalization of the transcription factor Yap1 following oxidative stress and then extended the approach to multi-compartment localization by examining two DNA repair proteins critical for the base excision repair pathway, Ntg1 and Ung1. Our findings demonstrate the utility of Q-SCAn for quantitative analysis of the subcellular distribution of multi-compartment proteins.

Keywords

Saccharomyces cerevisiae; localization; quantification; automated; compartmentalization; nuclei; mitochondria; fluorescence; image analysis

[*]To whom correspondence should be addressed. Tel: +1 404 727 0409; Fax: +1 404 727 2618; medpwd@emory.edu, Correspondence may also be addressed to Anita H. Corbett. Tel: +1 404 727 4546; Fax: +1 404 727 3954; acorbe2@emory.edu.

SUPPLEMENTARY INFORMATION

Supplementary information includes an appendix and five figures. Appendix S1 describes the technical details of how the Q-SCAn algorithm works and how to prepare it for a new system, and Figures S1–S5 diagram the flow of information through the CellProfiler pipelines so that the computational steps are easily visualized and understood.

Appendix S1. Technical details of implementing Q-SCAn.

INTRODUCTION

In eukaryotic cells, subcellular compartments are functionally defined by the proteins present within each compartment. While many proteins are localized to a single compartment, some proteins are localized to multiple compartments either constitutively or in response to cellular signals. For example, many transcription factors are localized to the cytoplasm until a signal triggers nuclear import (1,2). Such mobilization of proteins is an efficient strategy to alter local function in response to stimuli because transport of a preexisting pool of protein is more rapid than the *de novo* synthesis and localization of a comparable amount of protein. Other proteins simultaneously play roles in multiple compartments such as some DNA repair proteins that are localized to both the nucleus and mitochondria to maintain the integrity of the genomes in each of these cellular compartments (3).

Despite the biological significance of localizing proteins to multiple subcellular compartments, tools for quantifying the relative subcellular distribution of multi-compartment proteins have not been extensively developed. Many protein localization studies employ manual scoring from microscopy data, relying on the heterogeneity of the cell population and human visual detection to provide a useful threshold (4–7). However, these implicit thresholds are subjective and the process can be very labor-intensive. In addition, manual methods are only semi-quantitative as they are based on qualitative data. True quantification can be achieved by manually tracing the boundaries of the compartments of interest and then quantifying pixels within each compartment, but the laborious nature of this type of analysis means the number of cells that can be analyzed is effectively limited. Colocalization analysis (8), which has advanced greatly over the last decade and is widely available in image analysis software, is more suited to addressing questions about whether proteins and markers are spatially linked rather than about the distribution of a protein among distinct compartments. Photobleaching (9) and photoactivation techniques can be employed to examine dynamics (10); however, these techniques require highly specialized experimental setups and are also limited to larger cells amenable to such techniques. Biochemical fractionation techniques can also provide quantifiable compartmentalization information on a population of cells (4,11,12), but microscopy-based techniques are superior to fractionation because micrographs preserve the spatial relationships and yield information on the single cell level, not just the population average.

The limitations of the above techniques form a critical impediment to analyzing the steady-state distribution of proteins localized to multiple compartments. Development of advanced, automatable techniques that provide unbiased quantification of protein localization on a per-cell basis is becoming an active area of research. We have developed an approach to quantifying protein distribution among multiple compartments, which we term Quantitative Subcellular Compartmentalization Analysis (Q-SCAn). This microscopy-based method uses brightfield DIC images to identify cells, relies on a set of fluorescent markers to define subcellular compartments, and provides information about the amount of a protein of interest, marked by a third fluorescent reporter, within the identified compartments. By comparing the fluorescence intensities for each compartment, a localization index is calculated for each cell, yielding a quantitative measure of protein localization. Furthermore, the distribution of these localization indices can be compared between different cell types, conditions, and time points to address the regulation of protein localization.

Here we describe the development of Q-SCAn in *S. cerevisiae* and demonstrate its utility in measuring the single-cell localization of proteins by following the oxidative stress–induced relocalization of the transcription factor Yap1 (13). Next, we extend the approach to multi-compartment localization by examining the nucleomitochondrial base excision repair (BER)

protein Ntg1 (14). Finally, we apply the method to evaluate the localization of another nucleomitochondrial BER protein, Ung1 (15), which has not been previously analyzed in any quantitative manner. Our analysis of Ung1 provides new biological information about mechanisms of localization of Ung1 and thus insight into regulation of the BER pathway, demonstrating the utility of Q-SCAn for such studies. This work presents a novel method for quantifying the subcellular distribution of multi-compartment proteins which can be immediately put to use and extended without specialized equipment or programming experience.

RESULTS

Automated quantification of subcellular protein localization: Q-SCAn

To address a critical gap in the techniques available to rapidly and reproducibly provide quantitative information about protein distribution between multiple cellular compartments, we have developed a method termed Quantitative Subcellular Compartmentalization Analysis (Q-SCAn). To develop this system, we exploited the budding yeast *S. cerevisiae* and focused on developing a system that could be used to quantify protein levels in the nucleus and mitochondria.

We designed a dual reporter for *S. cerevisiae* that could be integrated into the genome to create a reporter yeast strain with constitutively labeled nuclei and mitochondria. The reporter encodes spectrally-distinct fluorescent proteins targeted to the nucleus and mitochondria via well-characterized targeting signals (Figure 1A). The nuclear reporter protein comprises the strong, artificial SV40 bipartite nuclear localization signal (NLS) (16) fused to the tandem dimer red fluorescent protein tdTomato (17). This reporter protein is expressed from the low-level *CYC1* constitutive promoter (18) and terminated by the *NUF2* terminator (19). The mitochondrial reporter protein is composed of the highly efficient *Neurospora crassa* Su9 mitochondrial targeting signal (MTS) (20) fused to the cyan fluorescent protein mCerulean (21). This reporter protein is expressed from the high-level *TEF1* constitutive promoter (18) due to the relative dimness of mCerulean as compared to tdTomato and is also terminated by the *NUF2* terminator (19) (Figure 1A). These reporters were integrated into the *S. cerevisiae LEU2* locus to create a constitutively-labeled yeast reporter strain.

To validate the localization of these fluorescent reporter proteins to the targeted compartments, we co-stained cells expressing either NLS–tdTomato or MTS–mCerulean with DAPI to label chromatin and mitochondrial nucleoids or MitoTracker Red to label mitochondrial proteins, respectively. As shown in the micrographs in Figure 1B and validated by colocalization analysis, the marker proteins localized to their intended subcellular compartments consistently and with high specificity, a necessary requirement for computer-assisted image analysis, whereas these standard dyes comparatively displayed a highly variable and nonspecific staining.

To carry out Q-SCAn, fluorescent micrographs of cells expressing the marker proteins were obtained (Figure 1C). The Q-SCAn method, which is implemented in the open source CellProfiler software package (the CellProfiler pipelines necessary to run Q-SCAn are available for download at http://www.biochem.emory.edu/doetsch/qscan.html), was then applied to the images collected as depicted in Figure 1D to: (i) identify the location of cells from the DIC image utilizing information from the marker channels; (ii) filter out cells that have poor marker fluorescence that would prevent robust identification of compartments; (iii) identify, within each cell, the location of nuclei and mitochondria using information from the tdTomato and mCerulean channels, respectively; (iv) subtract the nuclei and mitochondria from the cell to define the cytoplasm; (v) remove overlapping parts of nuclei

and mitochondria; and (vi) quantify mean GFP intensity within each cell compartment (Figure 1D). The result of the compartmentalization is shown in Figure 1E. A measure indicating the relative distribution of the protein, a localization index, is then constructed, where the mean nuclear GFP intensity is divided by the sum of the mean nuclear and mean mitochondrial GFP intensities. This analysis results in a measure ranging from 0 (100% mitochondrial) to 1 (100% nuclear) (Figure 1F). (See Appendix S1 and Figures S1–S5 for technical details of the analysis.)

To calibrate the system, we constructed and expressed localization sequence–fused GFP proteins targeted to the nucleus, NLS–GFP_2 (NucGFP) (16), and mitochondria, MTS–GFP_2 (MitoGFP), as well as one designed to remain in the cytoplasm, NES–GFP_2 (CytoGFP) (Figure 2A). The thresholds and corrections used in the algorithm were tuned such that the nuclear and mitochondrial GFP protein–expressing cells resulted in an exclusively nuclear or mitochondrial localization index, respectively (Figure 2B), though mitochondrial localization is somewhat less sharply-defined than nuclear localization. A protein which does not localize to either compartment, cytoplasmic GFP, has a neutral and diffuse localization index distribution. These data demonstrate that the nucleomitochondrial localization index is valid for quantifying proteins with distributions in between these two extremes.

Q-SCAn used to analyze nuclear localization

To assess the practical utility of Q-SCAn to examine a classical signaling paradigm for multi-compartment protein localization, the movement of a transcription factor from the cytoplasm to the nucleus (1,2), we analyzed the localization of the *S. cerevisiae* transcription factor, Yap1 (13). Under normal cellular conditions, Yap1 shuttles between the nucleus and the cytoplasm but shows diffuse, steady-state localization primarily to the cytoplasm, as the rate of nuclear export exceeds the rate of nuclear import (22). However, upon exposure to oxidative stress, although steady-state levels of Yap1 do not change significantly (23), Yap1 nuclear export is blocked, resulting in rapid nuclear accumulation (7,22).

We expressed Yap1–GFP in *S. cerevisiae* expressing the nuclear marker protein. As expected, in the absence of any oxidative stress (Figure 3A, no treatment), Yap1–GFP was diffusely localized throughout each cell (23). Cultures were then treated with a mild dose of hydrogen peroxide and samples were imaged within three windows of time following exposure (Figure 3A). Applying Q-SCAn using a nucleocytoplasmic localization index (cytoplasmic = 0, nuclear = 1), the rapid mobilization of Yap1 into the nucleus was readily apparent (Figure 3B). The time-course and extent of relocalization corresponds well with previously published work (7) as well as with manual scoring of the same data (Figure 3C). Q-SCAn also allowed us to obtain new biological information about the heterogeneity of the distribution of Yap1 in the population. Initially the variance in Yap1 localization is very wide, but the distribution quickly tightens during oxidative stress as nuclear localization increases. The comparison with manual scoring also allowed direct comparison of the efficiency benefits of using Q-SCAn. Analyzing the same dataset (from end of image collection to start of data analysis) of over 200 images manually required approximately 6 hours of working time while setting up and beginning the Q-SCAn analysis for the same number of cells required less than 30 minutes, with minimal interaction over the course of the analysis. With a small program we developed to fully automate the process, even this minimal interaction is eliminated (Appendix S1).

Q-SCAn used to analyze the dual-localized DNA repair protein Ntg1

To extend the utility of Q-SCAn beyond localization to a single compartment, we next analyzed a system where a protein is localized to two specific compartments. For this

purpose, we examined a DNA repair protein critical for the BER pathway, the yeast endonuclease III–like DNA *N*-glycosylase/AP lyase, Ntg1, which localizes to both the nucleus and mitochondria (14) to differing extents depending upon the DNA damage status of each genome (4).

To assess the utility of Q-SCAn for detecting differences in the distribution of a protein between the nucleus and mitochondria, we exploited previously-characterized mutants of Ntg1 with altered targeting to each compartment (5) as indicated in Figure 4A and compared their localization with wild type Ntg1. We expressed these Ntg1 localization sequence mutants (Figure 4A) in *S. cerevisiae* containing the Q-SCAn nuclear and mitochondrial reporter proteins. These cells were imaged and analyzed via Q-SCAn. Micrographs of representative fields of cells are shown in Figure 4B. Q-SCAn revealed that wild type Ntg1 is relatively evenly distributed between the nucleus and mitochondria, with most cells containing slightly more nuclear Ntg1 relative to mitochondrial Ntg1. Disrupting the MTS resulted in nearly complete loss of mitochondrial localization (Figure 4C). Altering both segments of the bipartite NLS within Ntg1 (NLS1 and NLS2) resulted in loss of nearly all nuclear localization of Ntg1 (Figure 4C). Consistent with a previous study that defined the contributions of NLS1 and NLS2 to Ntg1 localization (5), disruption of NLS2 also resulted in significant loss of nuclear localization, but, notably, Q-SCAn revealed that this Ntg1 variant retained some nuclear localization as compared to the NLS1/2 double mutant. These data demonstrate that Q-SCAn can be readily used to experimentally quantify the localization of nucleomitochondrial proteins with different distributions between cellular compartments, revealing even modest changes such as the difference between altering both NLS1 and NLS2 vs. NLS2 alone.

Application of Q-SCAn to define targeting signals within the DNA repair protein Ung1

Finally, to assess the utility of Q-SCAn to obtain novel biological insights, we analyzed another DNA repair protein, the *S. cerevisiae* uracil DNA-glycosylase, Ung1. Similar to Ntg1, Ung1 localizes to both the nucleus and mitochondria (24); however, neither the distribution of the protein between the two compartments has been analyzed, nor have the intracellular targeting signals been experimentally defined. The predicted nuclear and mitochondrial localization signal sequences within Ung1 were identified via the NUCDISC component of PSORT II (25) and iPSORT (26), respectively. As shown in Figure 5A, these predicted targeting motifs within Ung1 are arrayed in an overlapping manner similar to the organization of these sequences in Ntg1 (see Figure 4A).

Localization of wild type Ung1 reveals that this BER protein has a distinct intracellular distribution compared to Ntg1 (Figure 5B,C) as Ung1 displays greater nuclear concentration than Ntg1. This assessment can be made by comparing the distribution of localization indices for the two proteins (median, Ung1: 1.0 vs. Ntg1: 0.68). To extend the analysis and gain insight into the functional targeting signals in Ung1, we disrupted the three predicted localization sequences (MTS, NLS1, NLS2) within Ung1 by site-directed mutagenesis (Figure 5A). We compared the localization of these Ung1 variants to wild type Ung1 using Q-SCAn. Micrographs of representative fields are shown in Figure 5B. These results reveal that NLS1 is necessary and sufficient for nuclear localization of Ung1 (Figure 5C), defining the functional NLS within Ung1. NLS2 may have a minor contribution to nuclear localization, but the distributions of the NLS1 mutant and NLS1/2 double mutant are statistically identical. The Ung1 variant with the altered MTS lost all mitochondrial localization as would be predicted if this motif is a functional targeting signal (Figure 5C). These data demonstrate that Q-SCAn can provide novel information about the extent of intermediate shifts in protein localization that may not be readily apparent by visual inspection.

DISCUSSION

The goal of the work presented here was to develop a rapid and quantitative method that could be used to assess the relative amount of a protein present in multiple compartments. Our results demonstrate the utility of Q-SCAn for such studies. Given the automated and rapid data analysis feasible with Q-SCAn, biological questions that examine changes in the localization of a dual-compartment protein can be readily addressed quantitatively. For example, a change in compartment-specific localization in response to a cellular signal over time could be analyzed as presented here for Yap1. In addition, quantitative information regarding the contribution of intracellular targeting signals to specific cellular compartments, such as described here for the DNA repair proteins Ntg1 and Ung1, can be readily collected and analyzed. Thus, Q-SCAn expands the tools available to address questions of protein distribution in a quantitative manner. Furthermore, Q-SCAn has been implemented in such a way as to ensure that the method can be readily employed by those that wish to analyze any protein of interest.

This study also demonstrates how Q-SCAn can be employed to gather new biological information about a protein of interest. While accumulation of Yap1 within the nucleus upon oxidative stress is a well-established biological response (7,13,22), our analysis reveals information about the extent of nuclear localization with time. Furthermore, we employed Q-SCAn to define the functional localization sequences of the DNA repair protein Ung1, which is localized both to the nucleus and mitochondria (24). Our analysis reveals that the NLS1 sequence constitutes the functional classical NLS in Ung1. However, altering both predicted classical NLS motifs did not eliminate all nuclear localization, indicating that Ung1 likely exploits a non-classical nuclear import pathway to ensure access to the nucleus. Such a mechanism using dual pathways to access the nucleus has also been observed for Ntg1 (5). Thus, in addition to facilitating experiments through rapid and automated data analysis, the quantitative results obtained using Q-SCAn provide novel information that is not revealed through conventional qualitative scoring methods.

A major strength of Q-SCAn is that the approach has been developed so that it can be easily applied by a user without any need for highly specialized equipment or software. Q-SCAn employs the open-source CellProfiler software package (27). This package is user-friendly and highly modular, allowing for any aspect of the Q-SCAn algorithm to be modified for different circumstances or to couple with other analyses. The CellProfiler package is also under active development and improvement at the Broad Institute, and technical assistance is readily available if required (www.cellprofiler.org).

There are a number of points that must be taken into consideration when implementing Q-SCAn. First, a marker protein for the compartment or compartments of interest will need to be designed. The fluorescence spectrum of fluorescent markers should not overlap with the fluorescence spectrum of the analyzed protein. Here we selected tdTomato and mCerulean coupled with GFP based on the spectral properties of these fluorescent proteins (17). Another consideration is that, as described here, the localization examined is not that of the endogenous protein, but rather that of a fluorescently-tagged protein. Such tagged proteins are commonly used to obtain information about protein localization (28,29) but both the presence of the tag and the level of the tagged-protein relative to endogenous protein need to be taken into account when interpreting results. Fluorescence noise should also be monitored. Although several noise-removal methods are implemented in Q-SCAn, some noise still remains. As a result, as the target protein level approaches the noise level, the localization index will approach equality. Finally, care must be taken to ensure that the imaged cell fields are well-separated. While the cell-finding algorithm can readily separate

cells that touch, there can be difficulty in separating cell clusters, which could inadvertently be treated as a single cell.

Development of methods to analyze protein distribution is an active area of research. A recent publication employed a dye to mark the *S. cerevisiae* plasma membrane to quantify recruitment of YFP–Ste5 to the plasma membrane upon pheromone signaling (30). Using this approach, the authors were able to calculate both the pheromone dose-response for Ste5 recruitment to the membrane and the dissociation constant for Ste5 from the membrane. While elements of this quantitative approach are similar to Q-SCAn, there are some significant differences. These authors employed a dye to mark the target compartment, but such dyes are not readily available to specifically mark all cellular compartments. In addition, the method was implemented using a special-purpose software, Cell-ID (31). While this program, like CellProfiler, is open-source, significant expertise would be required to use or modify the program. Another key distinction from Q-SCAn is that the authors employed defocused brightfield images to identify cells. While this approach facilitates cell-finding, obtaining these images on a non-automated microscope would be laborious and employing such images could result in a loss of information about internal cellular morphology and cell fitness. Given the different biological questions addressed by the two approaches, recruitment of a protein to the membrane (30) and movement of proteins between intracellular compartments (this report), these two methods complement one another to obtain quantitative biological information.

As a general method, there are numerous ways that Q-SCAn could be developed and extended, which is facilitated by implementation in CellProfiler. For example, the cell-finding algorithm could be replaced to identify mammalian cells, and the compartment-finding algorithms could be adapted to different types of markers including immunofluorescence. A third fluorescent protein from the deep red spectral range such as mPlum (32) could be introduced to mark a third compartment of interest. More than three fluorescent protein compartment markers could be employed if spectral imaging/linear unmixing is used to separate the signals. The localization distribution information could also be coupled to other information, such as cell size, compartment morphology, or measures of the protein distribution within a compartment. With modifications, Q-SCAn could also be adapted to analyze localization within three-dimensional datasets (33). In addition to analyzing single images, Q-SCAn could further be employed to extract localization data from frames of a video, allowing quantitative analysis of the dynamics of protein relocalization within single cells. Q-SCAn could also have applications in diagnostics and therapeutics, as mislocalization of proteins is associated with disease processes including cancer, autoimmune disorders and degenerative disorders (34).

This study reports the development and utilization of Q-SCAn as a facile, quantitative analytical tool for providing broader and more detailed analysis of the localization of multi-compartment proteins when compared to the current approaches available.

Materials and Methods

Yeast strains, media, and growth conditions

S. cerevisiae strains used in this study are listed in Table 1. *S. cerevisiae* cells were cultured at 30°C in rich YPD medium (1% yeast extract, 2% peptone, 2% dextrose; and 2% agar for plates) or synthetic defined drop-out media for selection (uracil$^-$ine$^-$) and/or transcription induction (methionine$^-$). Plasmids or integrated constructs were transformed into cells by a modified lithium acetate method (35).

Plasmid construction

Plasmids used in this study are listed in Table 1. Both a nuclear marker gene (NLS–tdTom) and a mitochondrial marker gene (MTS–mCer) were constructed and inserted into an *S. cerevisiae* integration plasmid (pRS305) (36). Each marker gene was expressed from a constitutive promoter (low-level *CYC1* (18) and high-level *TEF1* (18), respectively, chosen to equalize the brightness of the marker protein) and terminated by a generic transcription terminator from the *NUF2* gene (19). The marker genes themselves are composed of a localization sequence fused to a fluorescent protein (NLS–tdTom: bipartite SV40 nuclear localization sequence (NLS) (16) and tdTomato (17); MTS–mCer: *Neurospora crassa* Su9 mitochondrial matrix targeting sequence (MTS) (20) and mCerulean (21)). The pRS305 *LEU2* gene contains a unique EcoRV site to linearize the plasmid and thus enhance integration efficiency. Localization of these reporters in *S. cerevisiae* was confirmed by co-staining with DAPI or MitoTracker Red CMXRos (Invitrogen) and performing colocalization analysis on the fluorescence micrographs (8,37). Mitochondrial and cytoplasmic GFP localization control plasmids were constructed by replacing the NLS of pNLS–GFP (16) with the Su9 MTS (20) or the nuclear export sequence (NES) of mammalian PKI (38), respectively. The Ung1–GFP plasmid was constructed by inserting the *UNG1* gene (ORF + 914 bp upstream) amplified by PCR from wild type *S. cerevisiae* (FY86), an in-frame C-terminal GFP (39), and *NUF2* terminator into pRS426 (40). The predicted classical NLS (25) and MTS (26) of Ung1 were mutated (NLS1: K18A, R19A; NLS2: K40A K41A; MTS: R5A, R6A) using the QuikChange II Site-Directed Mutagenesis Kit (Agilent). All constructs were verified by sequencing.

Confocal microscopy

All fluorescence micrographs were obtained using a Zeiss LSM 510 confocal fluorescence microscope using a Plan-Apochromat 100×NA Oil DIC objective. Each fluorescence channel was imaged sequentially, with the transmission brightfield DIC collected simultaneously with mCerulean. See Table 2 for parameters used. Fluorescence intensities from a 90.0 μm square area were encoded into a 1024×1024 pixel, 12-bit image file for near-optimal Nyquist sampling (41) and enhanced discrimination of fluorescence intensities, respectively. The laser dwell time was 1.60 μs/pixel. All pinholes were set to 168.00 μm (1 Airy unit for 543-nm laser line), resulting in an optical slice of ~0.8 μm. Expression of each fluorescent protein alone was used to control for crosstalk between the fluorescence channels. Greater than 100 cells were imaged for each condition. The median projections of ten uniform brightfield images and ten dark images per channel were used to correct images for shading and dark current, respectively.

Yap1–GFP hydrogen peroxide treatment

Overnight late-log phase (~1×10^8 cells/mL) cultures of *S. cerevisiae* cells expressing the Q-SCAn reporter and Yap1–GFP were washed twice with H_2O, resuspended in 1 mL H_2O, counted via hemocytometer, and adjusted to a density of $2–4 \times 10^7$ cells/mL. Cells were treated with 5 mM H_2O_2 and imaged by confocal microscopy both before treatment and within three time windows following the start of treatment: 1–10 min, 30–45 min, or 60–80 min of start of treatment. Cells were visually scored for nuclear only, cytoplasmic only, or nuclear and cytoplasmic Yap1–GFP localization.

Data analysis

Colocalization analysis of the marker proteins was conducted using the commercial software Volocity 5.6.2 (PerkinElmer). ImageJ 1.46r was used to export channels from the raw images and to compute the median shading and dark current correction images (42). CellProfiler 2.0 (Developer build) with custom plugins was used to process the images,

identify *S. cerevisiae* cells and compartments, and measure fluorescence intensities (27). CellProfiler Analyst 2.0 (r11710) was used to develop filtering thresholds for the algorithm (43). Statistical analysis was performed with Stata 11.2. The localization index for a single cell is the mean nuclear GFP intensity divided by the sum of the mean nuclear and mean mitochondrial GFP intensities, producing a value in the range of 0 (mitochondrial) to 1 (nuclear). Cells whose sum of intensities were below the noise threshold were excluded. Shifts in localization were assessed by the Kruskal-Wallis test and the post-hoc multiple comparisons test with correction for ties (44), with $\alpha = 0.05$.

Supplementary Material

Refer to Web version on PubMed Central for supplementary material.

Acknowledgments

We would like to thank the Emory Custom Cloning Core Facility and the Emory University Integrated Cellular Imaging Core of the Winship Cancer Institute (National Cancer Institute Cancer Center Support Grant P30CA138292), especially Debbie Martinson and Dr. Adam Marcus. We would also like to thank the members of the Doetsch and Corbett laboratories, especially Drs. Dan Swartzlander and Natalya Degtyareva, for their constructive feedback in designing these experiments and in the preparation of this manuscript. Finally, we thank the Imaging Platform at the Broad Institute for help with CellProfiler. This work was supported by the National Institutes of Health [grant numbers P01ES011163 to P.W.D., F31CA168272 to N.C.B.]. The content is solely the responsibility of the authors and does not necessarily represent the official views of the National Institutes of Health.

REFERENCES

1. Ye W, Lin W, Tartakoff AM, Tao T. Karyopherins in nuclear transport of homeodomain proteins during development. Biochim Biophys Acta. 2011; 1813(9):1654–1662. [PubMed: 21256166]
2. Kumar S, Saradhi M, Chaturvedi NK, Tyagi RK. Intracellular localization and nucleocytoplasmic trafficking of steroid receptors: an overview. Mol Cell Endocrinol. 2006; 246(1–2):147–156. [PubMed: 16388893]
3. Larsen NB, Rasmussen M, Rasmussen LJ. Nuclear and mitochondrial DNA repair: similar pathways? Mitochondrion. 2005; 5(2):89–108. [PubMed: 16050976]
4. Griffiths LM, Swartzlander D, Meadows KL, Wilkinson KD, Corbett AH, Doetsch PW. Dynamic compartmentalization of base excision repair proteins in response to nuclear and mitochondrial oxidative stress. Mol Cell Biol. 2009; 29(3):794–807. [PubMed: 19029246]
5. Swartzlander DB, Griffiths LM, Lee J, Degtyareva NP, Doetsch PW, Corbett AH. Regulation of base excision repair: Ntg1 nuclear and mitochondrial dynamic localization in response to genotoxic stress. Nucleic Acids Res. 2010; 38(12):3963–3974. [PubMed: 20194111]
6. Fernández-Cid A, Riera A, Herrero P, Moreno F. Glucose levels regulate the nucleo-mitochondrial distribution of Mig2. Mitochondrion. 2012; 12(3):370–380. [PubMed: 22353369]
7. Rowe LA, Degtyareva N, Doetsch PW. DNA damage-induced reactive oxygen species (ROS) stress response in *Saccharomyces cerevisiae*. Free Radical Biol Med. 2008; 45(8):1167–1177. [PubMed: 18708137]
8. Zinchuk V, Zinchuk O, Okada T. Quantitative colocalization analysis of multicolor confocal immunofluorescence microscopy images: pushing pixels to explore biological phenomena. Acta Histochem Cytochem. 2007; 40(4):101–111. [PubMed: 17898874]
9. Gonzalez-Gonzalez IM, Jaskolski F, Goldberg Y, Ashby MC, Henley JM. Measuring membrane protein dynamics in neurons using fluorescence recovery after photobleach. Methods Enzymol. 2012; 504:127–146. [PubMed: 22264532]
10. Gauthier A, Brandt R. Live cell imaging of cytoskeletal dynamics in neurons using fluorescence photoactivation. Biol Chem. 2010; 391(6):639–643. [PubMed: 20370315]

11. Mah W, Deme JC, Watkins D, Fung S, Janer A, Shoubridge EA, Rosenblatt DS, Coulton JW. Subcellular location of MMACHC and MMADHC, two human proteins central to intracellular vitamin B12 metabolism. Mol Genet Metab. 2013; 108(2):112–118. [PubMed: 23270877]
12. Pronsato L, Boland R, Milanesi L. Non-classical localization of androgen receptor in the C2C12 skeletal muscle cell line. Arch Biochem Biophys. 2013; 530(1):13–22. [PubMed: 23262317]
13. Moye-Rowley WS, Harshman KD, Parker CS. Yeast *YAP1* encodes a novel form of the jun family of transcriptional activator proteins. Genes Dev. 1989; 3(3):283–292. [PubMed: 2542125]
14. You HJ, Swanson RL, Harrington C, Corbett AH, Jinks-Robertson S, Sentürker S, Wallace SS, Boiteux S, Dizdaroglu M, Doetsch PW. *Saccharomyces cerevisiae* Ntg1p and Ntg2p: broad specificity *N*-glycosylases for the repair of oxidative DNA damage in the nucleus and mitochondria. Biochemistry. 1999; 38(35):11298–11306. [PubMed: 10471279]
15. Burgers PM, Klein MB. Selection by genetic transformation of a *Saccharomyces cerevisiae* mutant defective for the nuclear uracil-DNA-glycosylase. J Bacteriol. 1986; 166(3):905–913. [PubMed: 3519585]
16. Hodel MR, Corbett AH, Hodel AE. Dissection of a nuclear localization signal. J Biol Chem. 2001; 276(2):1317–1325. [PubMed: 11038364]
17. Shaner NC, Campbell RE, Steinbach PA, Giepmans BNG, Palmer AE, Tsien RY. Improved monomeric red, orange and yellow fluorescent proteins derived from *Discosoma* sp. red fluorescent protein. Nat Biotechnol. 2004; 22(12):1567–1572. [PubMed: 15558047]
18. Mumberg D, Müller R, Funk M. Yeast vectors for the controlled expression of heterologous proteins in different genetic backgrounds. Gene. 1995; 156(1):119–122. [PubMed: 7737504]
19. Kahana JA, Schnapp BJ, Silver PA. Kinetics of spindle pole body separation in budding yeast. Proc Natl Acad Sci USA. 1995; 92(21):9707–9711. [PubMed: 7568202]
20. Pfanner N, Muller HK, Harmey MA, Neupert W. Mitochondrial protein import: involvement of the mature part of a cleavable precursor protein in the binding to receptor sites. EMBO J. 1987; 6(11): 3449–3454. [PubMed: 2892669]
21. Rizzo MA, Springer GH, Granada B, Piston DW. An improved cyan fluorescent protein variant useful for FRET. Nat Biotechnol. 2004; 22(4):445–449. [PubMed: 14990965]
22. Yan C, Lee LH, Davis LI. Crm1p mediates regulated nuclear export of a yeast AP-1-like transcription factor. EMBO J. 1998; 17(24):7416–7429. [PubMed: 9857197]
23. Gulshan K, Lee SS, Moye-Rowley WS. Differential oxidant tolerance determined by the key transcription factor Yap1 is controlled by levels of the Yap1-binding protein, Ybp1. J Biol Chem. 2011; 286(39):34071–34081. [PubMed: 21844193]
24. Chatterjee A, Singh KK. Uracil-DNA glycosylase-deficient yeast exhibit a mitochondrial mutator phenotype. Nucleic Acids Res. 2001; 29(24):4935–4940. [PubMed: 11812822]
25. Nakai K, Horton P. PSORT: a program for detecting sorting signals in proteins and predicting their subcellular localization. Trends Biochem Sci. 1999; 24(1):34–35. [PubMed: 10087920]
26. Bannai H, Tamada Y, Maruyama O, Nakai K, Miyano S. Extensive feature detection of N-terminal protein sorting signals. Bioinformatics. 2002; 18(2):298–305. [PubMed: 11847077]
27. Kamentsky L, Jones TR, Fraser A, Bray M-A, Logan DJ, Madden KL, Ljosa V, Rueden C, Eliceiri KW, Carpenter AE. Improved structure, function and compatibility for CellProfiler: modular high-throughput image analysis software. Bioinformatics. 2011; 27(8):1179–1180. [PubMed: 21349861]
28. Huh W-K, Falvo JV, Gerke LC, Carroll AS, Howson RW, Weissman JS, O'Shea EK. Global analysis of protein localization in budding yeast. Nature. 2003; 425(6959):686–691. [PubMed: 14562095]
29. Wu B, Piatkevich KD, Lionnet T, Singer RH, Verkhusha VV. Modern fluorescent proteins and imaging technologies to study gene expression, nuclear localization, and dynamics. Curr Opin Cell Biol. 2011; 23(3):310–317. [PubMed: 21242078]
30. Bush A, Colman-Lerner A. Quantitative measurement of protein relocalization in live cells. Biophys J. 2013; 104(3):727–736. [PubMed: 23442923]
31. Gordon A, Colman-Lerner A, Chin TE, Benjamin KR, Yu RC, Brent R. Single-cell quantification of molecules and rates using open-source microscope-based cytometry. Nat Methods. 2007; 4(2): 175–181. [PubMed: 17237792]

32. Wang L, Jackson WC, Steinbach PA, Tsien RY. Evolution of new nonantibody proteins via iterative somatic hypermutation. Proc Natl Acad Sci USA. 2004; 101(48):16745–16749. [PubMed: 15556995]
33. Caster AH, Kahn RA. Computational method for calculating fluorescence intensities within three-dimensional structures in cells. Cell Logist. 2012; 2(4):176–188. [PubMed: 23538475]
34. Hung MC, Link W. Protein localization in disease and therapy. J Cell Sci. 2011; 124(Pt 20):3381–3392. [PubMed: 22010196]
35. Gietz RD, Woods RA. Transformation of yeast by lithium acetate/single-stranded carrier DNA/polyethylene glycol method. Methods Enzymol. 2002; Volume 350:87–96. [PubMed: 12073338]
36. Sikorski RS, Hieter P. A system of shuttle vectors and yeast host strains designed for efficient manipulation of DNA in *Saccharomyces cerevisiae*. Genetics. 1989; 122(1):19–27. [PubMed: 2659436]
37. Manders MM, Verbeek PJ, Aten JA. Measurement of co-localization of objects in dual colour confocal images. J Microsc. 1993; 169(3):375–382.
38. Wen W, Meinkotht JL, Tsien RY, Taylor SS. Identification of a signal for rapid export of proteins from the nucleus. Cell. 1995; 82(3):463–473. [PubMed: 7634336]
39. Anderson MT, Tjioe IM, Lorincz MC, Parks DR, Herzenberg LA, Nolan GP, Herzenberg LA. Simultaneous fluorescence-activated cell sorter analysis of two distinct transcriptional elements within a single cell using engineered green fluorescent proteins. Proceedings of the National Academy of Sciences. 1996; 93(16):8508–8511.
40. Christianson TW, Sikorski RS, Dante M, Shero JH, Hieter P. Multifunctional yeast high-copy-number shuttle vectors. Gene. 1992; 110(1):119–122. [PubMed: 1544568]
41. Scriven DRL, Lynch RM, Moore EDW. Image acquisition for colocalization using optical microscopy. Am J Physiol Cell Physiol. 2008; 294(5):C1119–C1122. [PubMed: 18353895]
42. Schneider CA, Rasband WS, Eliceiri KW. NIH Image to ImageJ: 25 years of image analysis. Nat Methods. 2012; 9(7):671–675. [PubMed: 22930834]
43. Jones T, Kang I, Wheeler D, Lindquist R, Papallo A, Sabatini D, Golland P, Carpenter A. CellProfiler Analyst: data exploration and analysis software for complex image-based screens. BMC Bioinformatics. 2008; 9(1):482. [PubMed: 19014601]
44. Zar, JH. Biostatistical Analysis. 4th ed.. Upper Saddle River, NJ: Prentice Hall; 1999.
45. Winston F, Dollard C, Ricupero-Hovasse SL. Construction of a set of convenient *Saccharomyces cerevisiae* strains that are isogenic to S288C. Yeast. 1995; 11(1):53–55. [PubMed: 7762301]

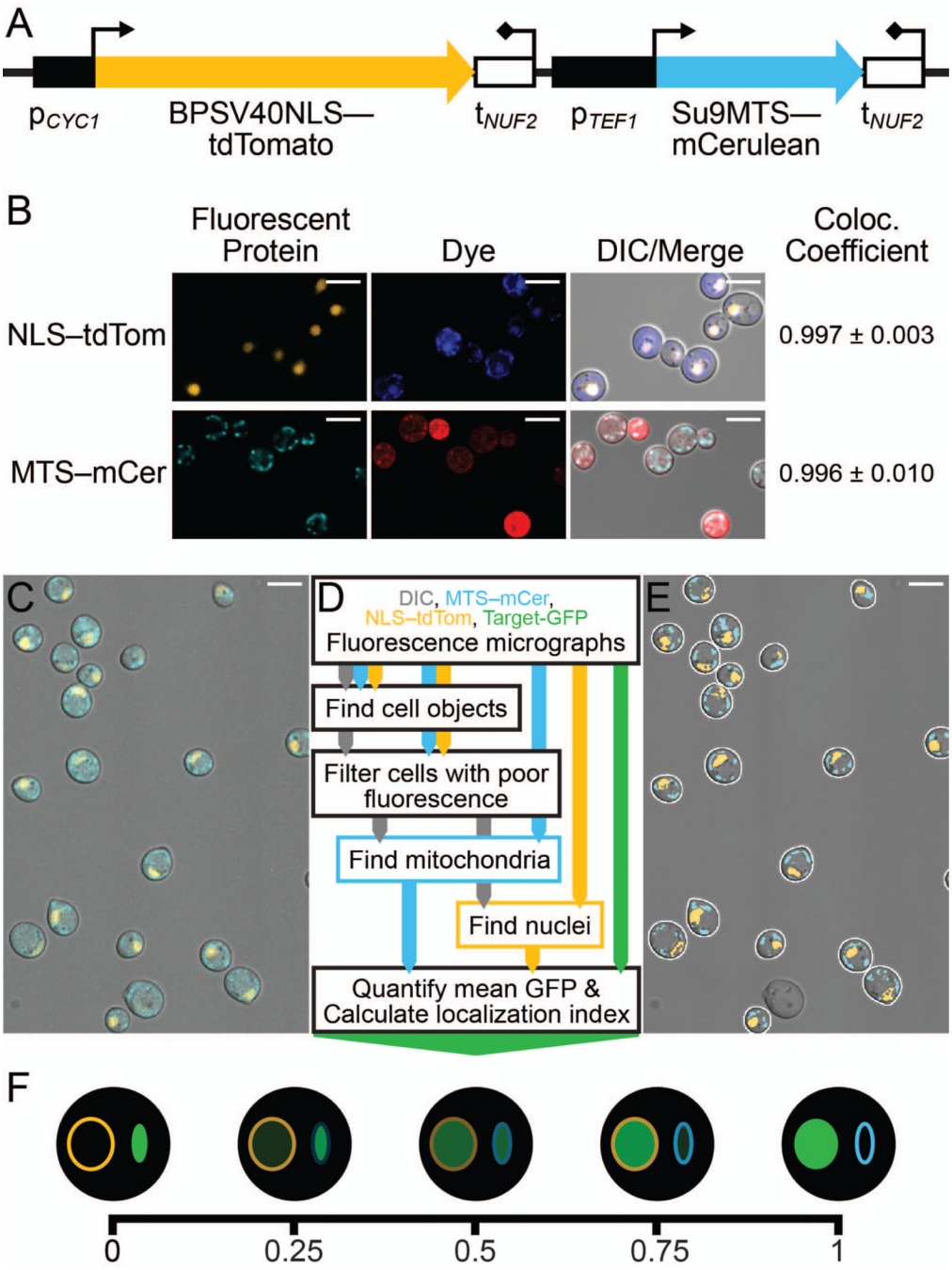

Figure 1.

Quantitative Subcellular Compartmentalization Analysis (Q-SCAn). **A)** Schematic of the tandem nuclear and mitochondrial marker protein construct, which is integrated into the *S. cerevisiae LEU2* locus as described in Results. **B)** The Q-SCAn marker proteins specifically and uniformly localize to their respective compartments. The nuclear and mitochondrial fluorescent marker proteins (NLS–tdTomato, MTS–mCerulean) were expressed independently in *S. cerevisiae* cells and co-stained with DAPI (Dye, upper panel) or MitoTracker (Dye, lower panel), respectively, and subjected to colocalization analysis to generate a colocalization coefficient (Coloc. Coefficient: Mean ± SD over 5 images). **C)**

Example merged image of cells co-expressing both fluorescent marker proteins. Scale bar is 5 μm. **D)** Diagram of the flow of information in Q-SCAn. **E)** Result of the compartmentalization of the sample image in **C**. Identified cells are outlined in white, identified nuclei are marked in orange, and identified mitochondria in cyan. Overlapping portions of compartments are excluded, and cells that do not have both markers expressed and visible in the optical slice are excluded. Scale bar is 5 μm. **F)** Schematic of the mito-nuclear localization index. The index is generated by dividing the mean nuclear GFP intensity by the sum of the mean nuclear and mean mitochondrial GFP intensities. A value of 0 indicates that all of the signal is in the mitochondria, while a value of 1 indicates that all of the signal is in the nucleus, as depicted by the cell diagrams (nucleus outlined in orange, mitochondria outlined in blue).

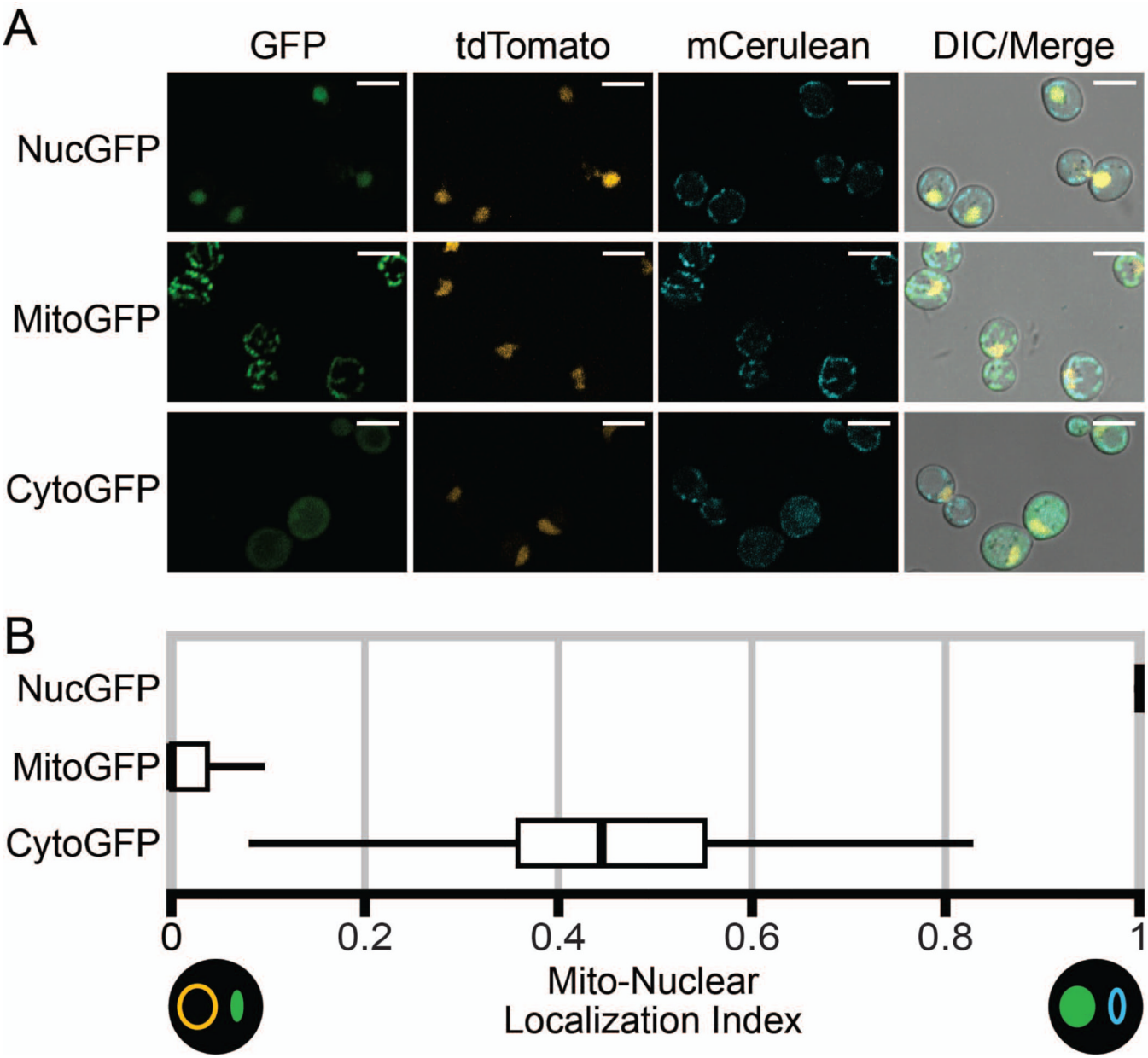

Figure 2.

Q-SCAn calibrated to detect distinct nuclear and mitochondrial localization. *S. cerevisiae* cells co-expressing integrated NLS–tdTomato and MTS–mCerulean, and nuclear, mitochondrial, or cytoplasmic GFP (NucGFP, MitoGFP, CytoGFP) were imaged. Greater than 200 cells were analyzed per experiment. **A)** Representative images of cells expressing a localized GFP. Scale bar is 5 μm. **B)** Quantification of the distribution of localization controls presented as mito-nuclear localization index (0 = mitochondrial to 1 = nuclear). Vertical black line indicates the sample median, white box the interquartile range, and horizontal black line the adjacent range.

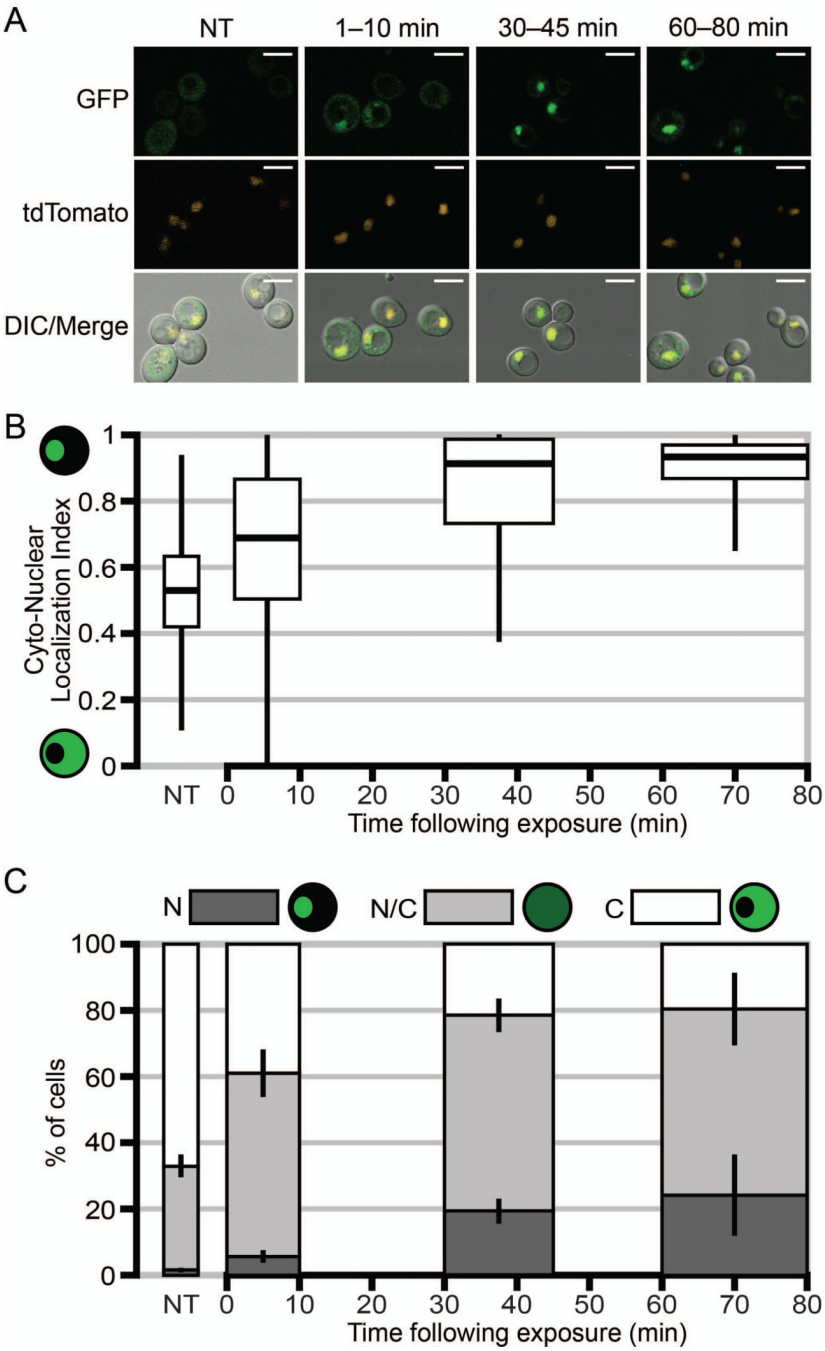

Figure 3.

Yap1–GFP redistributes to the nucleus under oxidative stress, as revealed by Q-SCAn. *S. cerevisiae* cells co-expressing integrated NLS–tdTomato and MTS–mCerulean, and Yap1–GFP were exposed to 5 mM hydrogen peroxide and imaged within three windows of time after exposure, 1–10 min, 30–45 min, and 60–80 min. Across three independent replicates, >200 cells were analyzed per time window. **A)** Representative images of cells expressing Yap1–GFP before treatment (No Treatment: NT) and within each time window following exposure. Scale bar is 5 μm. **B)** Quantification of the distribution of Yap1–GFP (0 = cytoplasmic to 1 = nuclear) within each time window following exposure. Horizontal black

line indicates the sample median, white box the interquartile range, and vertical black line the adjacent range. **C)** Percentage of cells visually scored for cytoplasmic (C, white), nuclear and cytoplasmic (N/C, light gray), or nuclear (N, dark gray) Yap1–GFP localization within each time window following exposure. Boundaries are mean ± SEM.

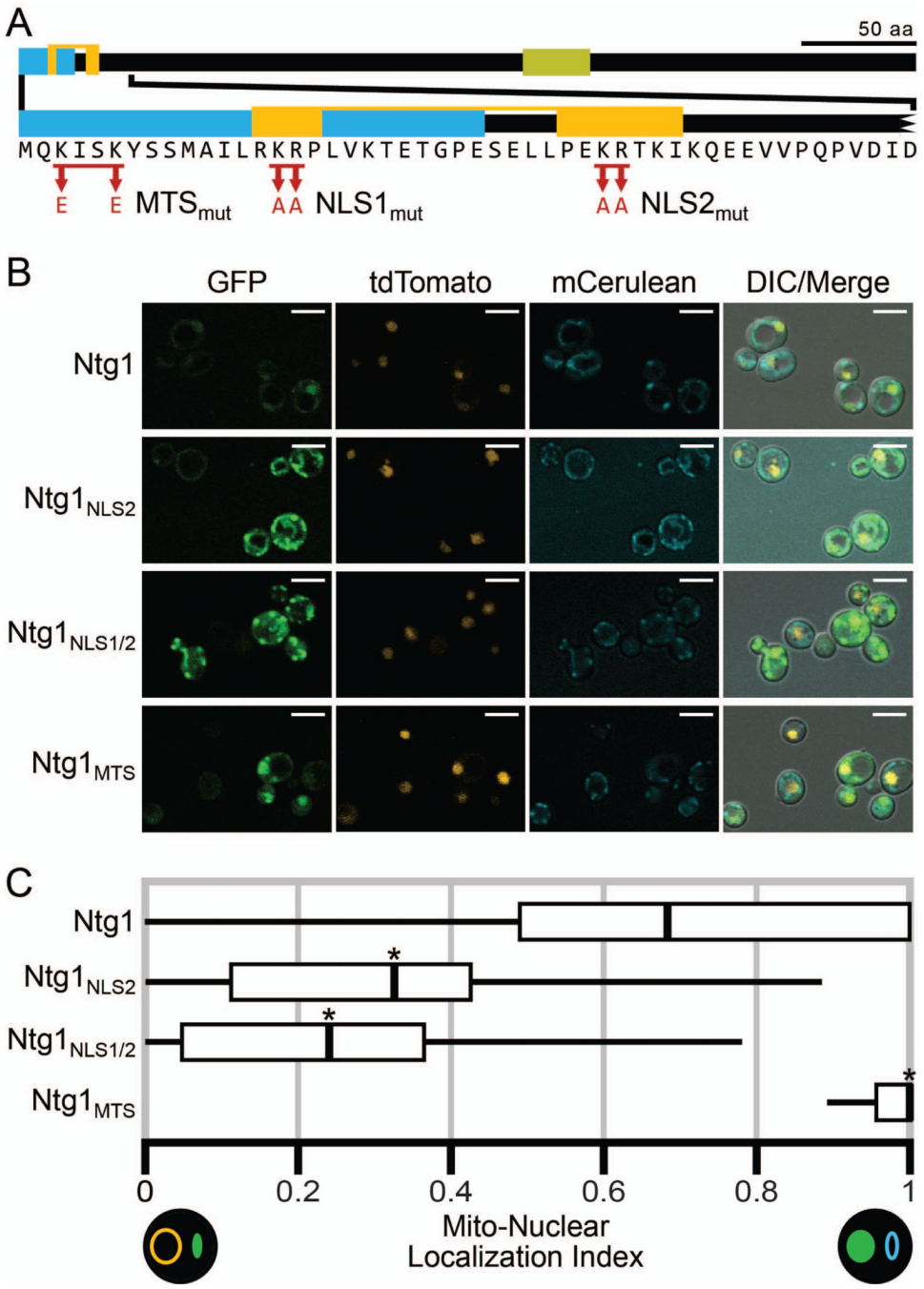

Figure 4.

Localization of Ntg1 analyzed by Q-SCAn. *S. cerevisiae* cells co-expressing integrated NLS–tdTomato and MTS–mCerulean, and an Ntg1–GFP variant were imaged. **A)** Schematic of Ntg1 showing nuclear localization motifs (NLS, orange), mitochondrial matrix targeting signal (MTS, blue), and catalytic site (yellow), indicating the amino acid changes introduced within each targeting signal. **B)** Representative images of cells expressing Ntg1–GFP variants. Scale bar is 5 μm. **C)** Quantification of the distribution of Ntg1–GFP fusion proteins (0 = mitochondria to 1 = nucleus). Vertical black line indicates the sample median, white box the interquartile range, and horizontal black line the adjacent range. Asterisk

denotes distributions determined to be significantly different from wild type Ntg1 ($p < 0.05$). Across three independent replicates, >350 cells were analyzed per variant analyzed.

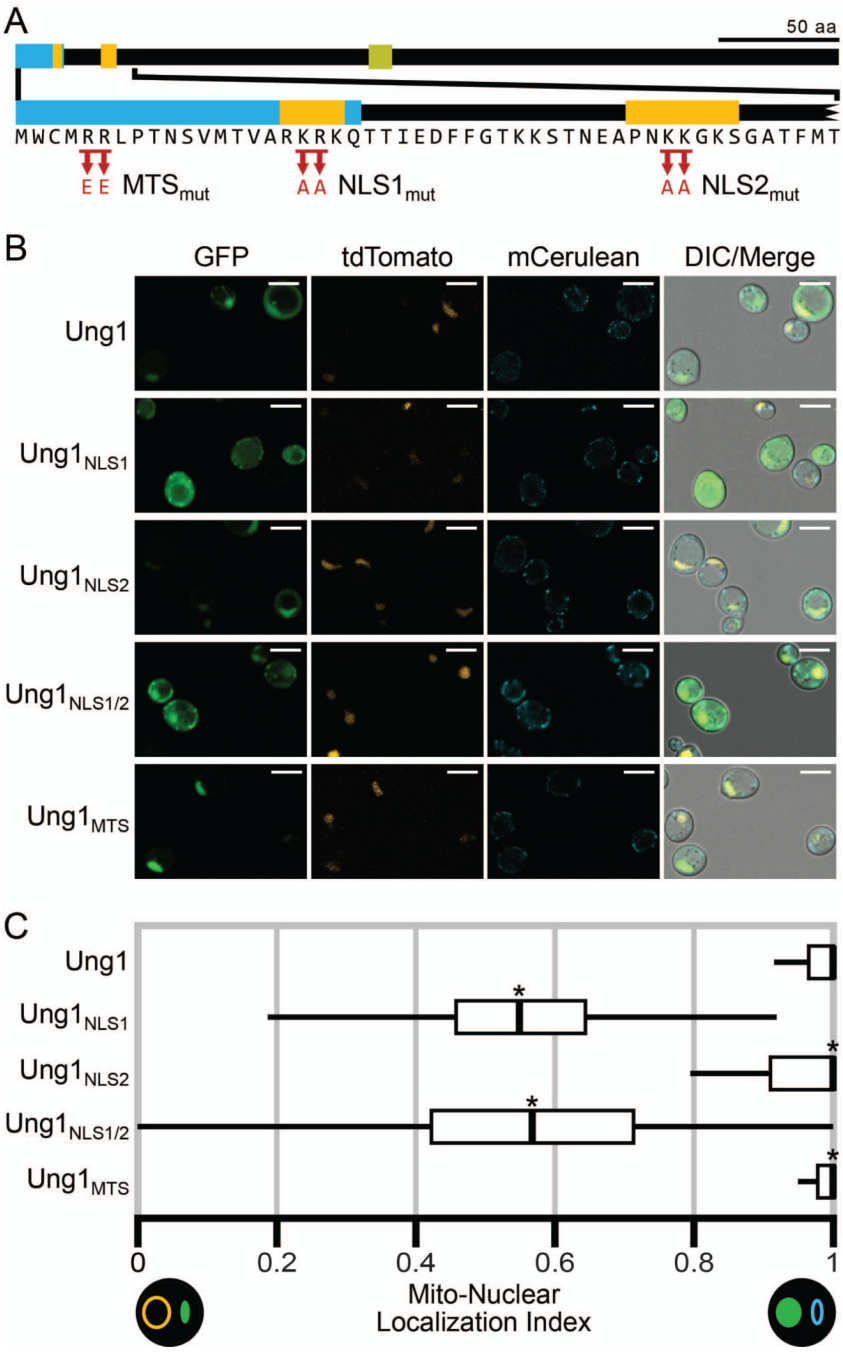

Figure 5.

Functional analysis of Ung1 targeting signals revealed by Q-SCAn. *S. cerevisiae* cells co-expressing integrated NLS–tdTomato and MTS–mCerulean, and an Ung1–GFP variant on a 2μ plasmid were imaged. **A)** Schematic of Ung1 showing its predicted nuclear localization signals (NLS, orange, identified via PSORT II (25)), mitochondrial matrix targeting signal (MTS, blue, identified via iPSORT (26)), and catalytic site (yellow), indicating the amino acid changes introduced within each putative targeting signal. **B)** Representative images of cells expressing Ung1–GFP variants. Scale bar is 5 μm. **C)** Quantification of the distribution of Ung1–GFP fusion proteins (0 = mitochondria to 1 = nucleus). Vertical black line

indicates the sample median, white box the interquartile range, and horizontal black line the adjacent range. Asterisk denotes distributions determined to be significantly different from wild type Ung1 ($p < 0.05$). Across three independent replicates, >250 cells were analyzed per variant analyzed.

Table 1

Plasmids and strains used in this study.

Name	Genotype	Ref
FY86 (ACY193)	*MATa ura3-52 leu2Δ1 his3Δ200*	(45)
Q-SCAn (DSC569)	*MATa ura3-52 his3Δ200 NLS–tdTom MTS–mCer*	This study
pRS305	*LEU2, AmpR*	(36)
pRS426	*2μ, URA3, AmpR*	(36)
pNLS–tdTom (pD0464)	p_{CYC1}*–BPSV40NLS–tdTomato, LEU2, AmpR*	This study
pMTS–mCer (pD0465)	p_{TEF1}*–Su9MTS–mCerulean, LEU2, AmpR*	This study
pQ-SCAn (pD0466)	p_{CYC1}*–BPSV40NLS–tdTomato,* p_{TEF1}*–Su9MTS–mCerulean, LEU2, AmpR*	This study
pNLS–GFP2	p_{MET17}*–BPSV40NLS–GFP–GFP, CEN, URA3, AmpR*	(16)
pMTS–GFP2 (pD0467)	p_{MET17}*–Su9MTS–GFP–GFP, CEN, URA3, AmpR*	This study
pNES–GFP2 (pD0468)	p_{MET17}*–NES–GFP–GFP, CEN, URA3, AmpR*	This study
pYap1–GFP	*YAP1–GFP, CEN, URA3, AmpR*	(7)
pNtg1–GFP	*NTG1–GFP, 2μ, URA3, AmpR*	(4)
pNtg1$_{NLS2}$–GFP	*ntg1*$_{NLS2}$*–GFP, 2μ, URA3, AmpR*	(5)
pNtg1$_{NLS1/2}$–GFP	*ntg1*$_{NLS1/2}$*–GFP, 2μ, URA3, AmpR*	(5)
pNtg1$_{MTS}$-GFP	*ntg1*$_{MTS}$*–GFP, 2μ, URA3, AmpR*	(5)
pUng1–GFP (pD0419)	*UNG1–GFP, 2μ, URA3, AmpR*	This study
pUng1$_{NLS1}$–GFP (pD0469)	*ung1*$_{NLS1}$*–GFP, 2μ, URA3, AmpR*	This study
pUng1$_{NLS2}$–GFP (pD0470)	*ung1*$_{NLS2}$*–GFP, 2μ, URA3, AmpR*	This study
pUng1$_{NLS1/2}$–GFP (pD0471)	*ung1*$_{NLS1/2}$*–GFP, 2μ, URA3, AmpR*	This study
pUng1$_{MTS}$–GFP (pD0472)	*ung1*$_{MTS}$*–GFP, 2μ, URA3, AmpR*	This study

Table 2

Confocal microscopy parameters.

	tdTomato	GFP	mCerulean	DIC
Excitation Laser Line (nm)	543 nm	488 nm	405 nm	405 nm
Laser Power (mW)	1.0 mW	15.0 mW	25.0 mW	25.0 mW
Laser Transmission (%)	10%	30%	65%	65%
Detected λ Range (nm)	>560 nm	505 – 545 nm	420 – 490 nm	—
Detector Gain (V)	750 V	725 V	750 V	260 V*
Amplifier Offset	−	−0.01	−0.03	0.00

*Sometimes had to be adjusted slightly to maintain an image solidly within the dynamic range.